Available online at www.sciencedirect.com

ScienceDirect

Scripta Materialia 82 (2014) 53–56

Scripta MATERIALIA

www.elsevier.com/locate/scriptamat

Control of microstructure and fracture toughness improvement of $NbSi_2/MoSi_2$ duplex lamellar silicides by TaC particles dispersion

Koji Hagihara,[a,*] Tatsuya Fushiki[a] and Takayoshi Nakano[b]

[a] *Department of Adaptive Machine Systems, Graduate School of Engineering, Osaka University, 2-1 Yamadaoka, Suita, Osaka 565-0871, Japan*

[b] *Division of Materials and Manufacturing Science, Graduate School of Engineering, Osaka University, 2-1 Yamadaoka, Suita, Osaka 565-0871, Japan*

Received 22 January 2014; revised 12 March 2014; accepted 24 March 2014
Available online 29 March 2014

The floating-zone melting method enabled the dispersion of TaC particles in a C40-$(Mo_{0.85}Nb_{0.15})Si_2$ single crystal. By annealing the C40 crystal, coarse $C11_b$ phases were formed around the TaC particles and the precipitation of the $D8_8$-$(Mo,Nb,Ta)_5Si_3C$ phase was also induced, in addition to the development of a C40/$C11_b$ lamellar microstructure. Such a microstructure containing TaC particles led to a reduction in the orientation dependence of the fracture toughness of duplex silicide crystals.

Keywords: Transition-metal silicides; Carbides; Toughness; Microstructure

Transition metal disilicides such as $C11_b$-$MoSi_2$ are promising candidates for use as ultrahigh-temperature structural materials that can potentially replace conventional materials in turbines [1–17]. The use of these materials could achieve higher operating temperatures for turbines, which would improve the thermal efficiency. However, the low-temperature fracture toughness and high-temperature strength (above 1200 °C) of transition metal disilicides, especially in their monolithic form, are inadequate for practical applications. One of the promising strategies to overcome these limitations is to combine different disilicides with favorable properties. From this viewpoint, Nakano et al. [8,9] have recently succeeded in developing $NbSi_2/MoSi_2$ composite crystals with fine lamellar microstructures. An oriented $NbSi_2/MoSi_2$ duplex lamellar crystal is obtained from a C40-structured $(Mo_{0.85}Nb_{0.15})Si_2$ single crystal grown by the floating zone (FZ) melting method and subsequent annealing of the C40 crystal at 1400 °C [9]. These duplex crystals showed superior high-temperature mechanical properties [13]. In addition, the development of lamellar microstructure was reported to increase the fracture toughness compared to that of C40 single crystal [12,16]. However, the maximum value is still ~3.2 $MPam^{1/2}$, hence further improvement of the fracture toughness is strongly desired. As one possibility, the dispersion of carbide particles is expected to increase the fracture toughness of the crystals by acting as barriers for crack propagation. However, since the superior mechanical properties of the $NbSi_2/MoSi_2$ duplex lamellar crystals are afforded by the control of the crystal orientation and the geometry of the lamellar microstructure [13,16], the carbide particles must be homogeneously dispersed in the C40 single crystals. In this study, the fabrication of C40 single crystals containing a carbide was attempted by the FZ method, focusing on TaC, WC and SiC carbides. The microstructure and mechanical properties of the carbide-containing $NbSi_2/MoSi_2$ duplex lamellar crystals were examined, and the effect of the carbide on the microstructure development and the mechanical properties was investigated.

In the experimental procedure, master ingots with a nominal composition of $(Mo_{0.85}Nb_{0.15})Si_2$ containing 5 at.% TaC, WC or SiC were first prepared by melting high-purity raw materials of Mo, Nb, Si and powdered carbides, with an average size of ~45 μm for TaC,

* Corresponding author. Tel.: +81 6 6879 7434; fax: +81 6 6879 4174; e-mail: hagihara@ams.eng.osaka-u.ac.jp

http://dx.doi.org/10.1016/j.scriptamat.2014.03.021
1359-6462/

~150 μm for WC and ~100 μm for SiC, in a plasma arc furnace. Using the mother alloys, C40 single crystals were grown by the FZ method at a growth rate of 2.5 mm h^{-1} under a high-purity argon gas flow. The mother ingots and seed crystals were rotated in the opposite directions to each other at 6 rpm during crystal growth in the FZ furnace to prevent significant clustering of the carbides and to induce their homogeneous dispersion in the melt. Some of the obtained single crystals were subsequently annealed at 1400 °C for 6–168 h to develop a lamellar microstructure. The constituent phases in the crystals were identified by X-ray powder diffraction analysis (XRD; Philips X-pert Pro) and energy-dispersive X-ray spectroscopy using a scanning electron microscope (SEM-EDS; JEOL JEM-6500F). The crystallographic orientation relationships between the constituent phases were examined by electron backscatter diffraction (EBSD) pattern analysis in the SEM. Rectangular specimens, with a size of 2 × 1 × 10 mm^3, were prepared and then subjected to three-point bending tests to evaluate the fracture toughness of the annealed specimens at room temperature (RT). The tests were conducted using an Instron-type testing machine with a cross-head speed of 0.005 mm min^{-1}. A notch was introduced into each specimen using a diamond wire cutter. Three kinds of specimens having lamellar microstructures with different geometries with respect to the loading axis and notch direction, called A, B and C, were prepared to examine the orientation dependence of fracture behavior. The details of the crystal geometry of the specimens are shown later in Figure 4, and are also given in our previous paper [16].

Figure 1(a) shows a typical microstructure of an as-FZ-grown crystal containing TaC carbides. By the X-ray Laue back-reflection method, it was confirmed that the obtained as-grown crystals were mainly composed of the single crystalline C40 matrix phase. In the C40 single crystal, the dispersion of TaC particles was observed as shown in Figure 1(a), though a certain amount of particle clustering could not be avoided. The same experiment was conducted on SiC-containing crystals. However, the SiC particles in a SiC-containing crystal floated and condensed in the upper region of the melt during the FZ process, hence the dispersion of SiC carbides in a C40 single crystal was not obtained. These differences are attributed to the difference in the density of the carbides. The density of SiC (~3.2 g cm^{-3}) is much lower than that of the matrix $(Mo_{0.85}Nb_{0.15})Si_2$ phase (~6.2 g cm^{-3}); thus, SiC easily floated in the melt. In contrast, the density of TaC (~14.6 g cm^{-3}) is higher than that of the melt. This indicates that the relative density of carbide particles with respect to the C40 matrix phase is an important factor for the fabrication of carbide-dispersed single crystals by the FZ method. From this viewpoint, WC (~15.6 g cm^{-3}) was also considered a suitable carbide. However, WC reacted significantly with the C40 matrix phase during solidification, hence its dispersion could not be obtained.

Figure 1(b)–(d) shows the typical microstructures of a single crystal after annealing at 1400 °C for 6, 24 and 168 h, respectively. A fine C40/$C11_b$ lamellar microstructure was developed by the annealing, and it was additionally found that the TaC particles were gradually covered by coarse $C11_b$ phases as increasing in the annealing period, as can be clearly seen in the higher magnification images in Figure 1(b) and (c). It should be noted here that many cracks formed in the as-FZ crystals during the mechanical polishing of the surface owing to its brittle nature, as shown in Figure 1(a). However, the number of cracks clearly reduced with increasing annealing period, i.e. with the development of a lamellar microstructure. This demonstrates the effectiveness of the lamellar microstructure in improving the toughness of a silicide crystal. Figure 1(e) shows the SEM backscatter electron image of a crystal annealed for 168 h at 1400 °C. After long-term annealing of this crystal, another phase was found to be precipitated, as shown by the white contrast. In some parts, the precipitates were observed to be extending from the TaC particles along the C40/$C11_b$ lamellar interface.

The change in the constituent phase caused by annealing was confirmed by XRD analysis. Figure 2(a) and (b) shows the powder X-ray diffraction profile of an FZ-grown crystal before and after heat treatment

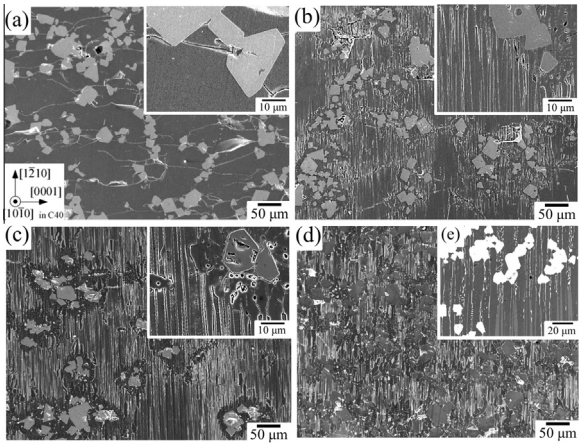

Figure 1. (a–d) SEM images showing the typical microstructures of (a) as-FZ grown $(Mo_{0.85}Nb_{0.15})Si_2$ crystal containing TaC carbides, and those after annealing at 1400 °C for (b) 6 h, (c) 24 h and (d) 168 h. The corresponding higher-magnification image is inset in the upper right-hand corners of (a–c). (e) SEM backscatter electron images of the crystal annealed at 1400 °C for 168 h.

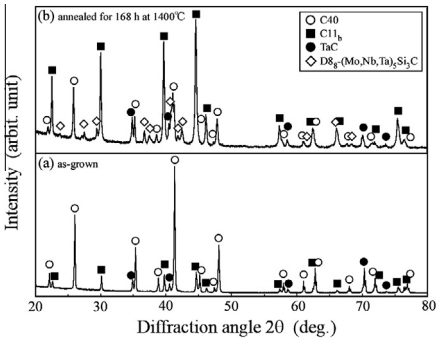

Figure 2. Powder X-ray diffraction profiles of TaC-particle-containing $(Mo_{0.85}Nb_{0.15})Si_2$ crystals: (a) as-FZ grown crystal, (b) crystal annealed at 1400 °C for 168 h.

at 1400 °C for 168 h. The as-grown crystal showed peaks derived mainly from the C40 matrix phase, together with peaks from TaC carbides. In addition, small peaks derived from $C11_b$ precipitates were also observed. This feature was different from those of non-TaC-added crystals [9]. The formation of the C40/$C11_b$ lamellar microstructure was in fact locally confirmed even in the as-FZ grown TaC-containing crystal in the OM observation. This suggests a possibility that the addition of TaC particles affected the precipitation behavior of the $C11_b$ phase, though the details have not yet been clarified. After annealing, on the other hand, the intensity of the peak derived from the C40 phase largely decreased, whereas that of the peaks derived from $C11_b$ precipitates increased. In addition, weak peaks derived from the $D8_8$-type phase were also observed, as indicated by open rhombuses. The lattice constants of the $D8_8$-type phase with a hexagonal unit cell were roughly estimated to be $a = 0.747$ and $c = 0.517$ nm from the XRD profile. It has been previously reported that interstitial C atoms stabilize the M_5Si_3 phase (M is a transition metal, such as Mo and Nb) as a $D8_8$-structured phase [18–20]. Thus, it is considered that small amounts of the TaC phase were dissolved in the C40 matrix phase, and saturated (Nb, Mo, Ta) atoms and C atoms promoted the precipitation of $D8_8$-M_5Si_3C. By the SEM-EDS analysis, the composition of the $D8_8$-type phase was roughly estimated to be $(Mo_{0.29}Nb_{0.33}Ta_{0.38})_5Si_3C$, though the amount of C could not be precisely determined by this method. $D8_8$ phases were predominantly precipitated around and inside the coarse $C11_b$ phases, but some of them were precipitated at the lamellar interface, as shown in Figure 1(e), suggesting that they precipitated with a distinct crystal orientation relationship with respect to the C40 matrix phase. This was confirmed by the SEM-EBSD pattern analysis. Figure 3(a) shows the SEM image of an annealed crystal viewed along $[10\bar{1}0]_{C40}$, and Figure 3(b) and (c) shows the corresponding orientation maps analyzed along $[0001]_{C40}$ for $C11_b$ and $D8_8$ phases, respectively. In addition, Figure 3(d) and (e) shows the orientation maps analyzed along $[8\,3\,\bar{11}0]_{C40}$, which is rotated 15° from $[10\bar{1}0]$ to $[11\bar{2}0]$ in a $[0001]$ zone axis. The crystal orientation of TaC carbides could not be determined since a clear EBSD pattern could not be obtained for them. When the crystal orientations were analyzed along $[0001]_{C40}$, most of the $C11_b$ phases with a lamellar microstructure were colored only by blue. This is because the $C11_b$ phases precipitated with respect to the C40 matrix phase as their close-packed $(1\,1\,0)_{C11b}$ and $(0\,0\,0\,1)_{C40}$ planes became parallel to each other [9]. In contrast, the coarse $C11_b$ phases that formed around TaC particles showed various different colors, indicating that they did not have a distinct orientation relationship with respect to the C40 matrix, different from the case of the lamellar-shaped $C11_b$ phases. When the crystal orientation was analyzed along $[8\,3\,\bar{11}0]_{C40}$, on the other hand, the $C11_b$ lamellae showed three colors: red, pink and purple. This is because they had three orientation relationships with respect to the matrix while maintaining the relationship of $(1\,1\,0)_{C11b}$ // $(0\,0\,0\,1)_{C40}$. These relationships are denoted as variants 1, 2 and 3 as follows [9]:

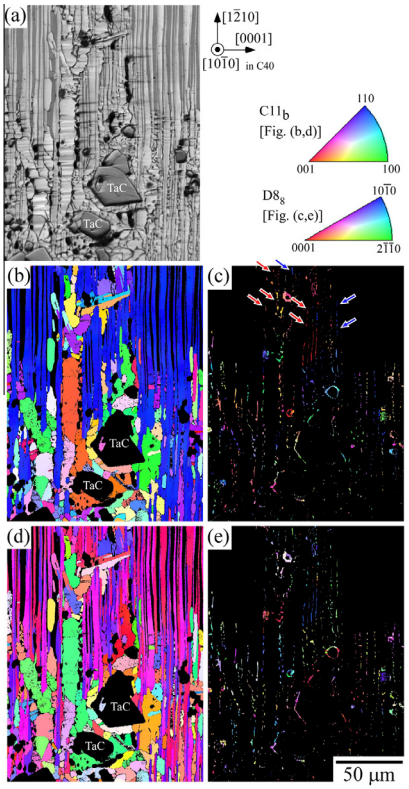

Figure 3. (a) SEM image of a specimen annealed at 1400 °C for 168 h observed along $[10\bar{1}0]_{C40}$. (b, c) Corresponding orientation maps along $[0001]_{C40}$ obtained by EBSD pattern analysis for the (b) $C11_b$ and (c) $D8_8$ phases. (d, e) Orientation maps obtained along $[8\,3\,\bar{11}0]_{C40}$ for the (d) $C11_b$ and (e) $D8_8$ phases.

$$\text{Variant 1}: (0001)_{C40} \,//\, (1\,1\,0)_{C11_b},\ [\bar{1}2\bar{1}0]_{C40} \,//\, [1\bar{1}0]_{C11_b},\ [10\bar{1}0]_{C40} \,//\, [001]_{C11_b} \quad (1)$$

$$\text{Variant 2}: (0001)_{C40} \,//\, (1\,1\,0)_{C11_b},\ [2\bar{1}\bar{1}0]_{C40} \,//\, [1\bar{1}0]_{C11_b},\ [0\bar{1}10]_{C40} \,//\, [001]_{C11_b} \quad (2)$$

$$\text{Variant 3}: (0001)_{C40} \,//\, (1\,1\,0)_{C11_b},\ [\bar{1}\bar{1}20]_{C40} \,//\, [1\bar{1}0]_{C11_b},\ [\bar{1}100]_{C40} \,//\, [001]_{C11_b} \quad (3)$$

The crystallographic features of the lamellar microstructure were identical to those observed for the non-added $(Mo_{0.85}Nb_{0.15})Si_2$ crystal.

On the $D8_8$ phases, those precipitated near to the coarse $C11_b$ phases showed various different orientation colors, as shown in Figure 3(b) and (d). The $D8_8$ phases precipitated on the C40/$C11_b$ lamellar interfaces were often colored red and blue in the orientation map analyzed along $[0001]_{C40}$, as indicated by arrows in Figure 3(c). This suggests the existence of orientation relationships with respect to the C40 matrix phase. By detailed analyses, the following two crystal orientation relationships were confirmed to be shown in many of the $D8_8$ phases formed on the lamellar interface with respect to the C40 matrix phase:

$$(0001)_{C40} \,//\, (0001)_{D8_8},\ [2\bar{1}\bar{1}0]_{C40} \,//\, [10\bar{1}0]_{D8_8} \quad (4)$$

$$(0001)_{C40} \,//\, (10\bar{1}0)_{D8_8},\ [2\bar{1}\bar{1}0]_{C40} \,//\, [0001]_{D8_8} \quad (5)$$

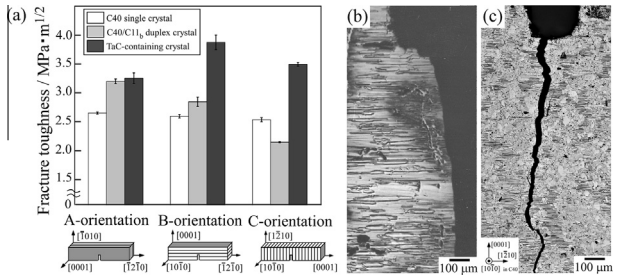

Figure 4. (a) Fracture toughness of TaC-containing $(Mo_{0.85}Nb_{0.15})Si_2$ crystals annealed at 1400 °C for 168 h, compared with those of non-added $(Mo_{0.85}Nb_{0.15})Si_2$ duplex crystals and $(Mo_{0.85}Nb_{0.15})Si_2$ C40-single-phase crystals, examined at RT. (b, c) Side-view images of the fractured surface of B-oriented specimen for (b) non-added duplex crystals and (c) TaC-containing crystals.

The crystal orientation relationship (4) has previously been reported by Geng et al. [19] in an Nb–Mo–Si system, but relationship (5) has been found for the first time in this study.

The fracture toughness of TaC-containing duplex lamellar crystals was examined by three-point bending tests, and the results were compared with those for non-added crystals [16]. The bending tests were conducted at three different loading orientations with respect to the lamellar interface, as depicted in Figure 4(a). At all loading orientations, the fracture toughness increased compared to that of non-added duplex crystal, as expected. Figure 4(b) and (c) shows side-view images depicting the crack propagation behavior in the B-oriented specimens of non-added and TaC-containing crystals, in which the lamellar interfaces were perpendicular to the loading orientation. TaC-containing crystals showed considerable crack deflection, whereas non-added crystals showed only little deflection. Crack deflection was frequently induced along the TaC carbides, demonstrating that the carbides effectively acted as barriers to crack propagation. In addition, the coarse $C11_b$ phase that formed around the TaC particles may have effectively contributed to crack-tip blunting, since the $C11_b$ phase is more ductile than the C40 matrix phase owing to the existence of many slip systems [2,7]. These features contributed to the increase in the fracture toughness. This toughness increase effect was more pronounced in the B and C orientations, in which the lamellar interfaces were perpendicular and parallel to the loading orientation, respectively. In particular, in the C orientation, there was a disadvantage with regard to the toughness in the duplex crystal; the value was lower than that of the C40 single-phase crystal since the cracks propagated easily along the lamellar interface [16]. However, this disadvantage could be improved by the addition of TaC particles.

To conclude, in this study, we successfully fabricated carbide-dispersed oriented $NbSi_2/MoSi_2$ duplex lamellar crystals by using TaC particles. The density of the carbide particles was found to be an important factor in the fabrication of carbide-dispersed C40 single crystals by the FZ process. The long-term annealing resulted in the TaC particles getting covered by ductile $C11_b$ phases in addition to the development of a fine lamellar microstructure. The addition of TaC particles led to an increase in the fracture toughness of the duplex crystal to some extent by inducing crack propagation deflection, and resulted in the reduction in orientation dependence of the toughness of the crystal. However, the highest value of the fracture toughness was still ~3.9 $MPam^{1/2}$, thus further work is required for this material to be suitable for practical use.

This work was supported by the "Advanced Low Carbon Technology Research and Development Program" of the Japan Science and Technology Agency. The authors wish to express their appreciation to Prof. H. Inui, Prof. K. Kishida and Prof. K. Yuge of Kyoto University, Japan and Prof. Y. Koizumi of Tohoku University, Japan, for their valuable comments on this research.

Supplementary data associated with this article can be found, in the online version, at http://dx.doi.org/10.1016/j.scriptamat.2014.03.021.

[1] A.K. Vasudevan, J.J. Petrovic, Mater. Sci. Eng. A 155 (1992) 1–17.
[2] K. Ito, H. Inui, Y. Shirai, M. Yamaguchi, Philos. Mag. A 72 (1995) 1075–1097.
[3] W.J. Boettinger, J.H. Perepezko, P.S. Frankwicz, Mater. Sci. Eng. A 155 (1992) 33–44.
[4] Y. Umakoshi, T. Nakano, E. Yanagisawa, et al., Mater. Sci. Eng. A 239–240 (1997) 102–108.
[5] K. Hagihara, T. Nakano, Y. Umakoshi, Scr. Mater. 38 (1998) 471–476.
[6] T. Nakano, M. Kishimoto, D. Furuta, Y. Umakoshi, Acta Mater. 48 (2000) 3465–3475.
[7] T. Nakano, M. Azuma, Y. Umakoshi, Acta Mater. 50 (2002) 3731–3742.
[8] T. Nakano, M. Azuma, Y. Umakoshi, Intermetallics 6 (1998) 715–722.
[9] T. Nakano, Y. Nakai, S. Maeda, Y. Umakoshi, Acta Mater. 50 (2002) 1781–1795.
[10] F.G. Wei, Y. Kimura, Y. Mishima, Intermetallics 9 (2001) 661–670.
[11] F.G. Wei, Y. Kimura, Y. Mishima, Mater. Trans. 42 (2001) 1349–1355.
[12] K. Hagihara, S. Maeda, T. Nakano, Y. Umakoshi, Sci. Technol. Adv. Mater. 5 (2004) 11–17.
[13] T. Nakano, K. Hagihara, Y. Nakai, Y. Umakoshi, Intermetallics 14 (2006) 1345–1350.
[14] Y. Kimura, M. Komiyama, Y. Mishima, Intermetallics 14 (2006) 1358–1363.
[15] K. Hagihara, T. Nakano, S. Hata, et al., Scr. Mater. 62 (2010) 613–616.
[16] K. Hagihara, T. Nakano, Acta Mater. 59 (2011) 4168–4176.
[17] K. Hagihara, Y. Hama, K. Yuge, T. Nakano, Acta Mater. 61 (2013) 3432–3444.
[18] H. Schachner, E. Cerwenka, H. Nowotny, Monatsh. Chem. 85 (1954) 245–254.
[19] T. Geng, C. Li, X. Zhao, H. Xu, C. Gao, Z. Du, Intermetallics 18 (2010) 1007–1015.
[20] J.-H. Kim, T. Tabaru, H. Hirai, A. Kitahara, S. Hanada, Scripta Mater. 48 (2003) 1439–1444.